



Measurement report: Characterization of uncertainties of fluxes and fuel sulfur content from ship emissions at the Baltic Sea

Jari Walden¹, Liisa Pirjola^{2,3}, Tuomas Laurila¹, Juha Hatakka¹, Heidi Pettersson⁴, Tuomas Walden¹, Jukka-Pekka Jalkanen¹, Harri Nordlund², Toivo Truuts⁵, Miika Meretoja⁶, Kimmo K. Kahma⁴

5 ¹Climate Research Program, Finnish Meteorological Institute, Helsinki, Finland

²Department of Automotive and Mechanical Engineering, Metropolia University of Applied Sciences, Vantaa, Finland

³Aerosol Physics Laboratory, Faculty of Engineering and Natural Sciences, Tampere University, Tampere, Finland

⁴Meteorological and Marine Research Program, Finnish Meteorological Institute, Helsinki, Finland

⁵Air Quality Management Department, Estonian Environmental Research Centre, Tallinn, Estonia

10 ⁶City of Turku, Turku, Finland

Correspondence to: Jari Walden (jari.a.walden@gmail.com)

Abstract. Deposition of gaseous compounds and nanoparticles from ship emissions was studied by micrometeorological methods at Harmaja in the Baltic Sea. The gradient method was used to measure fluxes of SO₂, NO, NO₂, O₃, CO₂, and N_{tot} (number concentration of nanoparticles). In addition, the fluxes of CO₂ were measured by the eddy covariance method.

15 Distortion of the flow field caused by obstacles around the measurement mast was studied by applying a computation fluid dynamic (CFD) model. This was used to establish the corresponding heights in the undisturbed stream, and the wind speed as well as the turbulent parameters at each of the established heights were recalculated for the gradient model. The effect of waves on the boundary layer was taken into consideration, because the Monin–Obukhov theory used to calculate the fluxes is not valid in the presence of swell. Uncertainty budgets for the measurement systems were constructed to judge the reliability of

20 the results. No clear fluxes across the air-sea nor sea-air interface were observed for SO₂, NO, NO₂, NO_x (= NO + NO₂) or O₃, while a negative flux was observed for N_{tot} with a median value of $-0.23 \times 10^9 \text{ m}^{-2} \text{ s}^{-1}$ and an uncertainty range of 31–41 %. For CO₂, while both positive and negative fluxes were observed, the median value was $-0.0036 \text{ mg m}^{-2} \text{ s}^{-1}$ with uncertainty ranges of 25–36 % and 30–60 % for the GR and EC methods, respectively. Ship emissions were responsible for deposition of N_{tot} while they had a minor effect on CO₂ deposition. The fuel sulfur content (FSC) of the marine fuel used in ships passing the

25 site was determined from the observed ratio of SO₂ and CO₂ concentrations. A typical value of $0.40 \pm 0.06 \%$, was obtained for FSC, which is in compliance with the contemporary FSC limit value of 1 % in the Baltic Sea Area. The method to estimate the uncertainty of FSC was found to be accurate enough for use with the latest regulations, 0.1 % (Baltic Sea Area) and 0.5 % (Global Oceans).



30 1 Introduction

The Baltic Sea, due to its nature as a relatively small inland sea with heavy ship traffic and a large population around the sea, is very sensitive to pollutants. Due to the very narrow and shallow strait of Kattegat in Denmark, the exchange of seawater between the North Sea and the Baltic Sea is limited. The load of phosphorus and nitrogen in the Baltic Sea mainly comes through the rivers. In addition, the airborne deposition of pollutants from the emissions of ships, and from industry, are becoming more and more important sources (Hongisto and Joffre, 2005). Ship emissions of most of the air pollutants except CO have decreased during 2006-2018, but greenhouse gas emissions from ships have remained stable throughout the period, regardless of the growth of ship transport reported in tonne kilometres (HELCOM, 2019). Ship emissions enter the sea mostly by indirect deposition of sulfur and nitrogen compounds through chemical conversion in the atmosphere (de Leeuw et al., 2003; Hongisto et al., 2005; Hongisto, 2014), or by direct deposition from the gas phase. The need for reduction of atmospheric pollutants in the emissions has been taken seriously within the International Maritime Organization (IMO), which launched the MARPOL agreement for reduction of ship emissions, Annex VI (IMO, 1997). The latest revision includes more stringent emission limits for NO_x and SO₂. In spite of these abatement regulations, the ship emissions of IMO registered vehicles and non-IMO registered vehicles show constant or slightly increasing trends for the compounds NO_x, SO₂, and PM_{2.5}, as well as a clearly increasing trend for CO. Once the stringent regulation for fuel sulfur content (FSC) in marine fuel came into power in 2014, the emissions of SO₂ and PM_{2.5} decreased rapidly at regional and global level (Johansson and Jalkanen, 2016; Johansson et al 2020; Seppälä et al. 2020).

The goal of this study was to measure fluxes of atmospheric pollutants from the ship emissions, to define the FSC from the ship emission plume and to characterise the uncertainty sources of the measurement result. The measurements took place at the Baltic Sea at the small island of Harmaja in the vicinity of the city of Helsinki during the summers of 2011 and 2012. The ship routes between the city of Helsinki and the cities of Tallinn, Stockholm and St. Petersburg pass by the measurement site. The exchange of the gaseous NO_x, SO₂, CO₂, O₃, and fine particles across the sea and -atmosphere surface layer was studied by micrometeorological methods. The fluxes of these compounds were measured by the gradient method and the eddy covariance method. In addition, concentration of methane was measured. The major sources of the pollutants were ship emissions, but also trans-boundary emissions as well as emissions from the sea and from the city of Helsinki contributed to the observed concentration levels of the pollutants. The FSC of the ships' marine fuel was determined from the measured concentrations of SO₂ and CO₂ (Cooper et al., 2005) to determine the compliance of the fuel used with the regulation. The ships passing the measurement site were identified by using AIS data (Jalkanen et al., 2009). This method has been demonstrated for defining the FSC in studies (Alföldy et al., 2013; Moldanova et al., 2013; Pirjola et al., 2014). Since recently, it has already been used as an indicator method for purposes of routine control by the authorities in some countries (Mellquist, 2018). The uncertainty of the flux and FSC measurements were estimated based on the performance of the analyzers and measurement probes for meteorological parameters, for FSC the uncertainty of defining the peak areas of emission plumes from the ships was also taken into account.



2 Theoretical background

2.1 Micrometeorological methods

65 The micrometeorological methods are used for measuring gas exchange across the surface layer (Kaimal and Finnigan, 1994);
of these the eddy covariance method (EC) and the gradient method (GR) are commonly used. The eddy covariance method is
a direct flux measurement method, while the gradient method is an indirect measurement method. In the eddy covariance
method the flux of a gas compound is measured by using fast sensors (response better than 10 Hz) to measure the fluctuation
of wind velocities and the concentration of chemical compounds. The gradient method overcomes the problems of fast analysis
70 of chemical compounds. On the other hand, this method requires that the atmospheric conditions are stationary, and it also
needs very accurate measurements of the parameters it uses (Businger, 1986), as well as the assumption of constant layer flux
(Dyer and Hicks, 1970). In this study both the GR and the EC methods were used. The gradient method was used for the gas
compounds (oxides of nitrogen, ozone, sulfur dioxide and carbon dioxide) as well as for nanoparticles. The eddy covariance
method was used to measure the flux of carbon dioxide. In the GR method the wind speed should be measured at different
75 heights, usually with conventional cup anemometers, while in the EC method the fluctuation of the 3-dimensional wind speed
is measured by a sonic anemometer. Short descriptions of both methods are given below, with more emphasis laid on the
gradient method.

$$F_s = -K_s \frac{\partial s}{\partial z} \quad (1)$$

where F_s is the flux of the scalar quantity s , K_s is the eddy diffusivity of s ; s means here the gas compounds and particles. The
80 gradient $\partial s / \partial z$ describes the mean concentration of s in the vertical direction z . By definition, the flux is opposite to the gradient,
which is positive towards the increasing concentration. The eddy diffusivity for a chemical compound c is calculated by
applying an assumption $K_c = K_h$, i.e. the eddy diffusivity of gas concentration is the same as that for heat. The eddy diffusivity
for heat transfer can be expressed as:

$$K_h = k \cdot u_* \cdot z / \phi_h \quad (2)$$

85 where ϕ_h is the dimensionless temperature gradient. Eq. (1) can now be rewritten with the help of Eq. (2) in the form

$$F_c = -\frac{k u_* z}{\phi_h} \frac{\partial c}{\partial z} \quad (3)$$

where k is the von Karman constant (≈ 0.4), u_* is the friction velocity, c is the concentration of the chemical compound, and
the dimensionless temperature gradient ϕ_h is defined as

$$\phi_h = \frac{kz}{\theta^*} \frac{\partial \theta}{\partial z} \quad (4)$$



90 Here θ is the potential temperature (Panofsky and Dutton, 1987) and θ^* ($= -\theta'w'/u_*$) is the scaling parameter for temperature. The dimensionless potential function, Eq. (4), can be written in a way similar to the momentum ϕ_m and for the concentration of a chemical species (gases and particulate matter) ϕ_i , respectively. The line above the symbol means the average of the quantity over time. Eq. (3) can be presented in the form

$$FC = -\frac{ku_*(c(z_2)-c(z_1))}{\left(\ln\left(\frac{z_2}{z_1}\right)-\psi_c(\zeta_2)+\psi_c(\zeta_1)\right)} \quad (5)$$

95 where $\psi_c(\zeta_2)$ and $\psi_c(\zeta_1)$ are the integral functions of Eq. (4) over the stability parameter ζ at heights z_2 and z_1 . The dimensionless gradient function Eq. (4) can be represented in the semi-empirical form of Businger and Dyer (Businger et al., 1971; Dyer, 1974), which is used here for the calculations. The stability parameter ζ is related to the Monin-Obukhov (M-O) length, L , according to the relation $\zeta = z/L$, where z is the height from the surface. Eq. (5) is valid in neutral ($\zeta = 0$) and unstable ($\zeta < 1$) conditions, but not in stable conditions ($\zeta \gg 1$) (Panofsky and Dutton, 1987).

100 In Eq. (5) the concentration difference at heights z_2 and z_1 is known from the measurements, but the friction velocity, the integral functions (ψ_c), and the stability parameter are unknown. To solve the turbulence parameters, a method proposed by Paulson (Paulson, 1970) was applied.

On the other hand, the sonic anemometer measures the wind velocity with the help of acoustic pulses that propagate along the path between the sound emitter and the receiver. The three-dimensional wind components, i.e. horizontal (u , v) and vertical
105 (w), are measured based on the changes in the acoustic signals along the fixed path lengths. The momentum flux F_m measured by the sonic anemometer can be calculated from the expression

$$F_m = \overline{\rho u'w'} = \rho u_*^2 \quad (6)$$

where ρ is the air density, u' and w' are the fluctuations of the wind speed components measured by the sonic anemometer, and u_* is the friction velocity. The friction velocity can be calculated from the surface stress according to

$$110 \quad u_* = (\overline{u'w'})^{1/2} \quad (7)$$

Once the friction velocity is calculated according to Eq. (7), the Monin-Obukhov length can be calculated:

$$L = \frac{\overline{T}u_*^3}{kgwT} \quad (8)$$

where T is the sonic temperature, T' is the fluctuation of the ambient temperature, and g is the acceleration of gravity. The M-O similarity theory states that the mean and turbulence variables in the surface layer are functions of height near the ground.
115 In a marine environment the M-O similarity theory has been found to be valid over slowly moving waves, which sufficiently resemble solid ground, but it fails in the presence of swell, i.e. waves that move faster than the wind (e.g. Drennan et al., 1999; Smedman et al., 1999). The effects of swell on the boundary layer are manifold (Högström et al., 2008, 2013, 2015), the most conspicuous being the absence of a vertical velocity gradient above a certain wavelength-dependent height. From the results



of Kahma et al. (2016) it can be deduced that the absence of wave components that are faster than the wind at 10 height is typically sufficient to ensure that the waves do not invalidate the M-O similarity theory.

Similarly to the momentum flux in Eq. (6) one can express the vertical flux of a gas compound, e.g. CO₂,

$$F_c = \overline{w' \rho'_c} \quad (9)$$

where ρ'_c is the mass density of CO₂ (mg/m³). The commonly used infra-red analysers measure the number density of CO₂, and to obtain the true mass density the fluxes have to be corrected for water vapour and heat fluctuations. The widely used correction method is the so called WPL method proposed by Webb et al. (1980), which is applied in this study.

2.2 NO-O₃-NO₂ chemistry

The chemical interconversion of the system NO - O₃ - NO₂ is well-known and described in the literature (Seinfeld and Pandis, 2012). In the atmosphere the reaction system NO - O₃ - NO₂ forms a cycle where the reaction forming NO₂, i.e., the reaction NO + O₃ is the reverse of the reaction for dissociating NO₂ to form NO, which takes place in the presence of sunlight (at wavelengths < 420 nm).

The chemical cycle in the NO - O₃ - NO₂ system is fast depending on the concentration of the compounds but also on the available sunlight (day/night time). The time scale (t) for vertical mixing can be estimated from the relation, $t = z/u^*$. With z as 10 m and the friction velocity between 0.1 to 0.5 m/s, the time scale for vertical mixing is 20 to 100 s. This is of the same order of magnitude as the time scale of the NO - O₃ - NO₂ system. Therefore, the assumption of vertical constant flux according to M-O theory is not valid. The approximation $K_h = K_c$ is not correct, and therefore the turbulent exchange coefficient K_c (Eq. (2)) must be modified. This problem has been discussed by several authors (Lenschow and Delany, 1987; Kramm et al., 1991; Vila-Guerau de Arellano et al., 1993; Duyzer et al., 1995). Lenschow and Delany (1987) constructed an analytical formulation for the flux profiles of the NO and NO₂ compounds as a function of height. Duyzer et al (1995) developed a correction procedure for the formula of Lenschow and Delany.

2.3 Estimation of the sulfur content in the marine fuel of the ships

The maximum sulfur content in the marine fuel used on the oceans is defined in the Annex VI of the MARPOL agreement (IMO, 2007). The agreement also defines the sea areas where a lower content of sulfur in the marine fuels must be used. These restricted sea areas, called SO_x Emission Control Areas (SECA) need to be approved by the countries in the proposed SECA. The Baltic Sea and the North Sea (IMO, 2007) form a SECA area, where the stringent sulfur limit for the marine fuels applies. In 2012, the EU updated the directive (Directive 1999/32/EU) to include the more stringent demands from MARPOL Annex VI (Directive 2012/33/EU). According to the MARPOL Annex VI the testing of sulfur content shall be in accordance with the ISO standard, which includes a set of key tests, e.g. to identify potential fuel issues where exceedances of emission may occur (ISO 8217:2012). According to ISO 8217 the standard method for the assessment of the sulfur content shall be in accordance



with the ISO 8754 (ISO 8754:2003). The main issue here is that the sample for the analysis of the sulfur content needs to be
150 taken from the bunker fuel at the harbour, not during the cruise.

A method that can be used to determine the FSC during the cruise is to measure the ratio of ΔSO_2 to ΔCO_2 from the emissions, either from the stack or from the ambient air. The ΔSO_2 and ΔCO_2 are the integrated peak concentrations of SO_2 and CO_2 when the background concentrations are subtracted i.e. $\Delta C = C_{\text{peak}} - C_{\text{bg}}$. By assuming that all sulfur in the fuel has been oxidized to SO_2 , the FSC can be calculated according to e.g. (10) (Pirjola et al. 2014):

$$155 \quad FSC (\%) = \frac{\frac{\Delta SO_2 (\text{ppb})}{10^3} M_S}{\Delta CO_2 (\text{ppm}) \cdot M_{CO_2}} \cdot EF_{CO_2} \cdot 100 = \frac{\Delta SO_2 (\text{ppb})}{\Delta CO_2 (\text{ppm})} \cdot 0.232 \quad (10)$$

where M_S and M_{CO_2} are the mole masses of S and CO_2 , and EF_{CO_2} is the emission factor for CO_2 . Here the value of 3.107 kg CO_2 per kg fuel burned was used (Petzold et al., 2008).

Eq. (10) yields lower limits for FSC (Williams et al., 2009) since a small part of the sulfur in the fuel, less than 6 % (Alföldy et al., 2013) or 0.7 % (Moldanova et al., 2013), might be emitted as SO_3 or converted to H_2SO_4 by homogeneous and
160 heterogeneous pathways in the atmosphere.

2.4 Uncertainty estimates

The uncertainty in the measurements is one of the most important issues to solve when analysing the results. The measurements are influenced by a number of error sources that need to be identified and quantified, e.g. the performance characteristics of gas and particle analyzers and the different probes and sensors used for the measurements. Besides the uncertainties associated
165 with the instruments, the EC and GR methods are very sensitive with respect to the topography and the atmospheric conditions. In particular, the stochastic nature of turbulence (Lenschow et al., 1994; Rannik et al., 2006) and the noise present in the measured signals cause random errors (Lenschow and Kristensen, 1985, Rannik et al., 2016), which are difficult to estimate. However, a number of error sources have been identified that have an influence on the results of flux measurement by the EC method (Businger 1986, Rinne et al 2000). The statistical error of an EC estimate is quite large even in a stationary flow. In
170 real-world meteorological conditions stationary situations are not common, and this dataset was not sufficiently large to provide a usable subset of such situations. Calculations showed that the uncertainty caused by the non-stationarity was in most cases considerably larger than the statistical error of a stationary sample.

Since the error sources that contribute to the uncertainty of the results cannot be completely corrected, there is always a residual component that needs to be included in the uncertainty budget. The residuals are estimated according to the best
175 knowledge available. The variance of the standard uncertainty can be expressed in the form (JCGM, 2008)

$$u_y^2 = \sum_{i=1}^n \left(\frac{\delta f}{\delta w_i} \right)^2 u_i^2 + 2 \sum_{i=1}^{n-1} \sum_{j=i+1}^n \frac{\delta f}{\delta w_i} \frac{\delta f}{\delta w_j} u_i u_j \rho_{ij}, \quad (11)$$

where the square root of u_c^2 is the combined standard uncertainty. It includes all the uncertainty components u_i (standard uncertainties) of the function f describing the measurement quantity in question for each of the parameters w_i associated with



the results of the measurements. The covariance term (the second term on the right-hand side) in Eq. (11) needs to be taken
180 into account when it is about the same order of magnitude as the independent part in Eq. (11). Once the combined standard
uncertainty has been determined, the expanded uncertainty U can be calculated according to $U = k \cdot u_c$. Here a factor of $k = 2$
was used representing the 95 % confidence level of a normal distribution. In the case of the gradient method the uncertainty
sources contributing to the fluxes associated with the method can be expressed by applying Eq. (2) to Eq. (11). For simplicity
the covariance terms in Eq. (11) have been ignored since they are of the second order of magnitude. The combined standard
185 uncertainty of the flux of a compound c can then be approximated in the form:

$$\frac{u_c(F_c)^2}{F_c^2} = \frac{u(u_*)^2}{u_*^2} + \frac{u(\Psi_h)^2}{\left(\ln\left(\frac{z_2}{z_1}\right) - \Delta\Psi_h\right)^2} + \frac{u(\Delta c)^2}{\Delta c^2} + \frac{u(z)^2}{\left(\ln\left(\frac{z_2}{z_1}\right) - \Delta\Psi_h\right)^2} \left(\frac{1}{z_1^2} + \frac{1}{z_2^2}\right) \quad (12)$$

The standard uncertainties are calculated according to Eq. (11) for each of the contributors in Eq. (12): the friction velocity,
the integral functions of the Businger-Dyer functions, the concentrations of gases and particles, as well as the measurement
heights. The estimated relative uncertainties for each of the contributing sources of uncertainty are presented in Supplementary
190 Table S1.

The combined standard uncertainty of the fuel sulfur content u_c (FSC) is estimated by applying Eq. (10) to Eq. (11), and it
can be expressed in the form:

$$\left(\frac{u_c(FSC)}{FSC}\right)^2 = \left(\frac{u(SO_2)}{\Delta SO_2}\right)^2 + \left(\frac{u(SO_{2,bg})}{\Delta SO_{2,bg}}\right)^2 + \left(\frac{u(CO_2)}{\Delta CO_2}\right)^2 + \left(\frac{u(CO_{2,bg})}{\Delta CO_{2,bg}}\right)^2, \quad (13)$$

where $u(SO_2)$ and $u(CO_2)$ are the standard uncertainties of the measured SO_2 and CO_2 concentrations at the peak area
195 concentration, while $u(SO_{2,bg})$ and $u(CO_{2,bg})$ are the standard uncertainties of the background concentrations.

3 Measurements and data analysis

3.1 The measurement site and the meteorological parameters

The first measurement campaign at Harmaja (60°06′18.166″N, 24°58′28.808″E) started on July 13 after installation of the
measurement instruments, and it ended on October 12, 2011. The second campaign started on July 7 and ended on August 20,
200 2012. The isle of Harmaja is a pilot station located in the Gulf of Finland, about four kilometres from the city of Helsinki in
Finland. The ship routes both from Tallinn to Helsinki and from Stockholm to Helsinki pass by the isle of Harmaja at distances
of 1 km and 100 – 200 m, respectively, as shown in Fig. 1. Fig. 1 also shows the modelled NO_x emissions.

The measurement station (Fig. 2) was set up in an old military fire control tower made of steel and concrete. All the
measurement instruments were installed inside the tower, while measurement probes and sampling inlets were installed at
205 different heights in a mast beside the tower. The height of the mast was 9 m, and it was standing on a breakwater 3.5 m above
mean sea level (MSL). The measurement probes were installed at different heights to get an extensive view of the
meteorological quantities. Cup anemometers by Vaisala (WAA 15 cup anemometers, Vaisala, Finland) measured the wind



speed while the turbulence parameters were measured by an ultrasonic anemometer by METEK (Ultrasonic Wind Sensor uSonic-3 Scientific, METEK GmbH, Germany). Pt-100 sensors measured the ambient temperature. The cup anemometers
210 were installed at three different heights, 12.2 m, 10.9 m, and 9.9 m above MSL. The sonic anemometer was installed at the top
of the mast at a height of 12.9 m, and the temperature probes were installed at heights of 12.3 m, 11.0 m, and 10.0 m. The
sampling intakes for the gaseous compounds were installed at two different heights, 12.58 m and 9.98 m. The inlets (stainless
steel) for particle measurements were installed at 8.0 m and 10.0 m. Next to this mast the official weather mast of the FMI
(Fig. 2) was standing, equipped with a cup anemometer (WAA 15 wind vane, Vaisala, Finland) and a wind direction vane by
215 Vaisala (WAV-15) at a height of 16.6 m. The current sea level was measured as a 30 min average with reference to MSL. The
measurement heights of the probes used in the calculations are from the current sea level.

3.2 Instrumentation

The atmospheric concentrations of ozone, oxides of nitrogen and sulfur dioxide were measured simultaneously by conventional
gas analyzers intended for ambient air quality measurement. Two identical analyzers of each gas were used to detect the
220 concentration at the two measurement heights (12.58 m and 9.98 m). The sampling tubes at each altitude were made equal in
length. PTFE (Polytetrafluoroethylene) was used as tube material, since it is an inert material for each of the gaseous pollutants.
The measurement method for ozone was the UV-photometric method (EN 14625:2012), and it was performed with APOA-
360 analyzers by Horiba, Japan. For nitrogen oxides (NO_x) the chemiluminescence method was used (EN-14211:2012) and
the measurements were performed with the AC31M analyzer by Environnement S.A., France. The AC31M analyzer was
225 constructed as a two-channel instrument that measures the concentration of NO and NO₂ simultaneously. For sulfur dioxide
the UV-fluorescence method (EN-14212:2012) was used and measured with a TEI 43 CTL analyzer by Thermo Environment.
LI-7000 by Licor was used for the EC method to measure the concentration of CO₂ and H₂O. Picarro G2301 by Picarro Inc
measured the concentration of CO₂, CH₄ and H₂O. Results of the LI-7000 and the Picarro G2301 were also used for calculating
the CO₂ flux with the GR method. The water content of the air has an effect on the measurements of gaseous compounds like
230 CO₂ using the absorption of infrared light (IR) at specific wavelengths. To avoid the interference from water vapor on the CO₂
analyzers the results obtained by the EC were corrected as proposed by Webb (Webb et al., 1980). In the case of the GR
method, this correction was not applied since it is the same for both heights, and does not change the concentration difference
between the two heights.

Particle number concentration and size distribution were measured by two ELPIs (Electrical Low Pressure Impactor, Dekati
235 Ltd.) (Keskinen et al., 1992); ELPI1 measured at 10.0 m and ELPI2 at 8.0 m height. The measurement principle of both ELPIs
was the same: particles were first charged and then classified into 12 stages according to their aerodynamic diameter, in the
size range of 7 nm–10 μm. Both ELPIs were equipped with a filter stage (Marjamäki et al., 2002), and ELPI1 additionally with
an extra stage designed to enhance the particle size resolution for nanoparticles (Yli-Ojanperä et al., 2010). The cut-off
diameters were 0.016 (additional stage, only in ELPI1), 0.030, 0.056, 0.093, 0.156, 0.264, 0.385, 0.617, 0.954, 1.610, 2.410,



240 4.04 (only in ELPI2) and 9.97 μm . The mass concentration of particles smaller than 1 μm (PM_{10}) was calculated by assuming the particles to be spheres with a density of 1000 kg/m^3 .

The strategy for the air quality measurements in 2012 was different, and it included measuring concentrations of NO , SO_2 , CO_2 , O_3 , and particles at one height, and CO_2 fluxes by the EC method. The NO_x analyzer was a modified version of a single channel analyzer, Thermo 42 CTL by Thermo Environment. The modification was made by bypassing the NO_2 converter and
245 the solenoid valve, increasing the flow rate by choosing an orifice which allowed a flow rate of up to 2 l/min, and by using the shortest integration time. The purpose of the modification was to make the analyzer faster for detecting the emission peaks of the ships, but for the NO gas only. The SO_2 analyzer was also a modified version from TEI 43 CTL by Thermo Environment. The purpose of modification was the same as in case of NO_x analyzer: to make it faster for detecting ship emissions. The O_3 and CO_2 analyzers and the particle analyser (ELPI1) were the same as in the 2011 campaign.

250 3.3 Calibration of the instruments

The temperature probes (Pt-100) were calibrated at the FMI in the calibration laboratory for meteorological quantities. The wind speed anemometers were serviced (cleaned and the ball bearings changed) in the same laboratory. The gas analyzers were calibrated in the reference calibration laboratory at the FMI before and after the field campaign. The calibration laboratory is responsible for the tasks of the national reference laboratory on air quality, and it conducts the calibrations of the air quality
255 analyzers and calibration facilities in Finland. The laboratory maintains the traceability of the calibration to the SI units, and it is accredited according to ISO 17025:2005 for all measured gas compounds except CO_2 . The dynamic dilution method by accurate gas sources was used for the calibration (Haerri et al. 2017). The calibration concentrations were selected to cover the expected measurement ranges for each of the gas components.

Besides the SO_2 molecules also other gas compounds such as nitrogen oxide and nitrogen dioxide can be excited by the
260 same wavelength as SO_2 giving a response to the SO_2 -analyzer. The influence of NO and NO_2 compounds on the response of the SO_2 -analyzer was tested in the laboratory. Known concentrations of NO and NO_2 gases were injected into the SO_2 -analyzer to define the response function for both NO and NO_2 . The results of the SO_2 -analyzer were then corrected accordingly.

Analyzers were also calibrated at the measurement site during the campaign using a field calibration unit similar to that in the laboratory. Both ELPIs were factory calibrated and serviced. Zero setting and HEPA filtration tests were performed before
265 and after each measurement period. Based on the parallel measurements of the ELPIs on 30.8.2011 and 2.9. 2011 correction factors were inferred for ELPI2, separately for each stage (see Supplementary material). This ensures that the results are correct within the stated uncertainty and are comparable with the other similar measurements.

3.4 Data acquisition systems and data analysis

The data acquisition systems consisted of several components. The meteorological measurements were collected and stored
270 by a Milos 500 system (by Vaisala). The ambient air quality gas analyzers were connected to a data collection system EnviDas



2000 (by Envimetria, Israel), the sonic anemometer and the LI-7000 were connected to a fast data acquisition system; Picarro G2301 used the system provided by the manufacturer, and the ELPI software was used for the collection of particle data.

275 The times, in EET (+2 UTC), of the different data acquisition systems were synchronized during each calibration and maintenance event. The final adjustment of all data sets at each of the altitudes was made manually from the time series so that the obvious peaks coincided. Data collection for the EC method was performed at 1 Hz time resolution. In the case of the GR method, data was collected as 15 second and one minute averages, while the total number concentration of particles in the size range of 7-1000 nm (N_{tot}) and PM_{10} were collected at 10 second intervals. The meteorological data from the official weather mast were collected as 10 min averages. A consistent data set was formed as 30 min averages from the synchronized individual data acquisition systems.

280 The first target for the data analysis was to achieve accurate and good quality continuous time series for the gaseous compounds and particles at each of the measuring heights. Secondly, the turbulence parameters (M-O length, stability parameter, friction velocity) were needed for calculating the transfer coefficients K_m and K_c , the dimensionless gradient, and their integral functions for heat and momentum, and for calculating the fluxes of the chemical compounds and fine particles. The friction velocity and the M-O length, which were calculated from the data obtained by the sonic anemometer, were used
285 as input parameters for the GR method. The benefit of this was to reach better agreement with the flux parameters.

3.5 Measurements on R/V Aranda

In 2012 measurements were also made on the Finnish research vessel Aranda during two days. The ship was kept stationary at a point approximately 2 km SSW from the measuring mast at Harmaja, with no islands between Harmaja and the ship. The bow of the ship was equipped with a sonic (Metek USA-1), an open path LI-7500 and an enclosed path LI-7200 at two heights
290 (10 and 16 m) for the measurement of the CO_2 , H_2O , momentum and heat fluxes. During the measurements the ship's bow was kept within +/- 20 degrees into the wind direction. The sonic measurements were corrected for ship motions with a motion sensor MRU6, according to Drennan et al. (1994). In this study the measurements from the sonic and enclosed path LI-7200 at the height of 16 m were used, and the calculated fluxes were corrected for water vapour fluctuations according to Webb et al. (1980). The partial pressure of CO_2 in the surface water at a depth of 4 m obtained from the ship's flow-through system
295 was measured continuously with an equilibrator and a LI-6262. The measurements were transformed to *in situ* water temperature according to Takahashi et al. (1993). All the LI-CORs were calibrated against 0, 364, and 700 ppm CO_2 gases.

4 Results

4.1 General overview

300 Environmental factors, e.g. the fire control tower, caused challenges with regard to the measurement signals. Though the measurement probes were installed at different heights above the top of the tower the measurement signals were affected by disturbances in the flow field. Therefore a computational fluid dynamic (CFD) program OpenFOAM (version 7) by the



OpenFOAM Foundation (OpenFOAM, 2020) was used to determine the amount of distortion and the required correction. OpenFOAM is a C++ based open source software developed mostly, but not exclusively, for CFD. The airflow around the shoreline and the measuring structure was modelled using steady, incompressible, single-phase potential flow. The simulation
305 covered a volume 80 m long, 40 m wide and 30 m high around the measurement area.

Fig. 3a illustrates the calculated wind field isopleths at a wind speed of 9 m/s over the open sea area, and it shows how the flow field is disturbed around the measurement mast. Based on this calculation we determined for each measurement height the corresponding height over the open sea. The heights at the measurement masts for wind speed measurements were reduced from 16.63 m, 12.88 m, 12.18 m, 10.88 m and 9.88 m, to 15.5 m, 11,1 m, 10.2 m, 8.6 m and 7.2 m, respectively. Similarly, the
310 heights of the sample intakes were reduced from 12.88 m, 12.58 m, 10 m, 9.88 m and 8 m down to 11,1 m, 10.7 m, 7.38 m, 7.2 m and 4.7 m, respectively. The correction for the wind speed was calculated from different simulations varying the wind speed and comparing the calculated results at the measurement mast with the open sea area. These calculations show that a linear relationship for the wind distortion at the measurement mast as compared with the open sea area was good enough to correct the observed wind speed measurement at all heights. The recalculated wind speed profiles (six profiles, cases 1 to 6)
315 at each of the corrected measurement heights are presented as averages over short periods (2 to 3 hours) in the wind sector to the open sea, i.e. $180^\circ \leq \text{WDIR} \leq 330^\circ$. The data were roughly classified into three categories: code 1, the M-O theory is valid (no swell), code 2, the M-O theory is most probably valid (moderate swell), and code 3, the M-O theory is not valid (dominant swell). In Fig. 3b the wind speed profiles (cases 1 to 6) are presented in situations where the M-O theory is valid (code 1) and where the M-O theory is not valid (code 3). In Fig. 3c the ambient air temperature profiles are calculated from the same
320 situations as the wind profiles. In Fig. 3d the wind rose at the height of 15.5 m shows the patterns of prevailing wind sectors with wind speed ranges.

As an example, Fig. 4a-b depicts the time series of 1-minute-averaged concentrations of the measured gas compounds at 10 m altitude during the first campaign. The sharp peaks in the concentrations of nitrogen monoxide are very striking. In a detailed examination the duration of the emission peaks from the ships were of the order of a few minutes. Where there was a
325 peak in the NO concentration, a negative peak was also detected in the ozone concentration due to the fast reaction producing NO₂. This was observed within seconds after the emission from the ship into the atmosphere. The changes in the concentrations of NO, NO₂ and O₃ were equal, i.e. the change in the concentration of NO took place according to the stoichiometric balance.

The concentration of sulfur dioxide was very low, but clearly distinguishable peaks, with a maximum of 28 ppb, were observed in the data. These peaks originated from the passing ships. The ship peaks were also seen in the CO₂ data, but the
330 short-term variation of the CO₂ concentration might be larger than the contribution from the ship emissions (Fig. 4b). When looking at the particulate concentrations N_{tot} and PM₁ (Fig. 4d), interesting features can be observed. Ship peaks can be clearly distinguished; however, the background levels of N_{tot} and PM₁ were highest on 28 August in the morning when the wind blew from the south, and lowest during the period from noon on 28 August to 10 AM on 30 August, when the wind came from the west over the ocean (Fig. 4c). The 96 h backward trajectory analysis of Flextra by NILU (Stohl et al., 1995) also showed that
335 in the measurement period before the noon of 28 August an air mass carrying anthropogenic pollutants was transported through



central Europe and arrived in Helsinki (Fig. 5a). The average background particle concentrations stayed rather constant at $\sim 2.7 \times 10^3 \text{ \#/cm}^3$, whereas the PM_{10} increased from $\sim 4 \text{ \mug/m}^3$ to $\sim 11 \text{ \mug/m}^3$ during 12 hours. This indicates that also larger particles were transported. In fact, this is obvious from Fig. 6, which presents the average number size distribution (Fig. 6a) as well as the volume size distribution (Fig. 6b) of background particles in the evening of 27 August, at noon on 28 August just before the clean air mass arrived, and in the afternoon of 28 August. During the next two days (noon 28.8. to noon 30.8.) the air trajectories came from the west, mostly over the Atlantic and the Baltic Sea, carrying clean air to Helsinki. Although the particle number concentration was higher, $3.6 \times 10^3 \text{ \#/cm}^3$, due to the larger number of the smallest particles, they did not have an effect on the volume size distribution.

4.2 Concentration roses

Figure 7 presents the maximum values for the concentrations of each gas compound and the particle number within wind sectors of 10° at both measurement heights. These results are in good agreement with the ones based on the sum of the measured concentrations, thus showing the cumulative contribution from different wind sectors at the measurement point (not shown). For NO_x and SO_2 , similar patterns were observed indicating the ship routes in sectors 90° to 120° , 150° to 180° , and 270° to 300° . In addition, there is a clear difference in concentrations between the heights: the higher concentrations were mostly at the highest measurement level. In the case of oxygen compounds ($= \text{O}_3$ and $\text{O}_3 + \text{NO}_2$) and CH_4 the patterns were more evenly distributed. In the case of CO_2 and N_{tot} there is an indication of the ship routes, but also of the influence of the city of Helsinki.

4.3 Fluxes

The eddy diffusivities K_h and K_m describe the conditions of the turbulent mixing for momentum and heat. The latter describes also the behaviour of the gaseous compounds and particles, as explained in section 2.1. In Fig. 8, the eddy diffusivities K_h and K_m at the measurement level of the sonic anemometer are presented as a function of stability.

From Fig. 8a, b, and d, it is also evident that in this data swell occurs mostly in the far unstable conditions, and only in a few cases in stable conditions, while the situations with no swell occur in this data in near the neutral conditions. The rose figure (Fig. 8c) for wind speed and friction velocity shows a clear dependence on the wind direction. There is clearly a linear relationship between the average wind velocity and the friction velocity in the sectors where the wind arrives over an open sea area, whereas non-linear behaviour is seen towards the northern sector (345° to 45°), where there are more obstacles. The gradient function for momentum also has a significant spread around the Businger - Dyer gradient function in the wind sector from 150° to 270° .

The calculation of the turbulence parameters by the GR method is sensitive to the platform itself, the atmospheric conditions, and the wind profile, which should not be disturbed by obstacles or swell. At the Harmaja site in 2011, the measurement mast was directly supported by the fire control tower (Fig. 2), which caused disturbances in the flow field. Therefore, the CFD program was used to determine the amount of distortion and the required correction. In addition, the results of the sonic anemometer (friction velocity and stability parameter) were used in calculating the fluxes. Before the



calculation it is necessary to evaluate the measured concentration differences between the measurement heights, with their uncertainty limits. The uncertainty limit was calculated for each type of the analyzers based on its performance characteristic. These were tested either by a testing laboratory (Thermo 43CTL, Environnement AC31M, APOA 360) or during the campaign. In the case of ELPI both instruments were injected with parallel samples to obtain a calibration formula as described in Supplementary Fig. S1. In the case of the CO₂ analyzers both types of instrument, LI-7000 and Picarro G2301, are commonly used in the Global Atmosphere Watch (GAW/WMO) programme, and test results were collected from the specifications requirements of the programme. The uncertainty limits for the gas and particle analyzers are presented in Supplementary Fig. S2. The calculated concentration differences between the measurement heights, and their uncertainty limits, are presented in Supplementary Fig. S3 for each of the gaseous compounds and for nanoparticles. Based on the analysis, the concentration differences for CO₂ and N_{tot} exceeded the uncertainty limit, indicating that the calculated fluxes are acceptable; they are presented in Fig. 9. In Fig. 9a the CO₂ fluxes by the GR and EC methods are presented. The fluxes of CO₂ and N_{tot} by the GR method along with their uncertainties (Eq. 12) in the wind sector between 150° to 270° and with no swell (codes 1 and 2) are presented in Fig. 9b and Fig. 9c, respectively. The fluxes of CO₂ and N_{tot} as a function of wind direction are presented in Fig. 9d.

The CO₂ fluxes calculated by the two methods (GR and EC) are in fairly good agreement (Fig. 9a). For most of the time the CO₂ flux was positive (upward) (Fig. 9b), while the flux of N_{tot} was mostly negative (downward) (Fig. 9c). Generally, positive CO₂ fluxes are common in the winter, and occasionally in the summer after the spring algae bloom, since CO₂ is less soluble in the warming sea water. In the Baltic Sea, however, the blue-green algae bloom extends the biological active season, and the positive fluxes in coastal regions are mainly caused by frequent upwelling events (e.g. Lehmann and Myrberg, 2008, Norman et al. 2013). The CO₂ flux by the EC method and the partial pressure of CO₂ in seawater were measured at the same time as the R/V Aranda measurements in late July 2012; this pin down the upwelling event (Fig. 10). As shown in Fig. 9d, the CO₂ fluxes show only a weak dependence on the wind direction, while in the case of N_{tot} there is a clear dependency, with the largest negative fluxes in the sectors containing ship routes (150-270°). Assuming that the constant flux layer extends to the height of the ships' chimneys, profile measurements of the compounds indicate that the deposition of nanoparticles towards the sea surface is most probably caused by ship emissions. The CO₂ emission peaks from the ships last only minutes, and in this area ships pass roughly once in an hour; it may be estimated that the contribution of the ship emission is of the order of 1 % of the observed average flux of CO₂. The weak dependence within the sectors containing ship routes suggests that the direction of the CO₂ flux in a marine environment is mainly controlled by the partial pressure of CO₂ in the seawater.

The uncertainty of the observed fluxes were calculated according to Eq. (12). The uncertainty sources of the measurement results for fluxes by the gradient method are presented in more detail in Supplementary Table S1. Though the wind speed was corrected based on the results of the CFD, there is always a residual that cannot be corrected. The influence of the uncertainty in the wind speed is included as a single component in Table S1. To estimate the uncertainty of the CO₂ flux measurements by the EC method we calculated the reactive difference (F1-F2)/F2 between the flux estimate F1 when the trend in the wind speed was removed and the estimate F2 when this trend was not removed. In a sufficiently long, perfectly stationary sample



there should be no trend, and the difference should vanish. In most of the samples the difference was significantly larger than the expected statistical variability of the EC estimate of a perfectly stationary sample. Rather than estimating accurately the uncertainty, the standard deviation of the relative difference was chosen as a simple proxy. For the momentum flux it was 30
405 %, and for the CO₂-flux 60 %. This wide uncertainty range is typical in real meteorological situations and explains the scatter of the EC estimates in e.g. Fig. 10. The analysis of the uncertainty follows the guideline provided by the Joint Committee for Guides in Metrology (JCGM, 2008). Based on the analysis, the relative expanded uncertainty for the flux measurements of CO₂ and nanoparticles by micrometeorological method is presented in Table 1 at two meteorological conditions: stationary and not stationary.

410 **4.4 Fuel sulphur content**

The FSC was determined in the measurement campaigns in both 2011 and 2012. The two campaigns differed from each other in the measurement strategies, but also in the data collecting frequency, once a minute in 2011 and every 15 s in 2012. In both cases, the data acquisition system calculated the averages over the data collecting time. It became very clear that the frequency of once a minute was too low in order to see accurate emission peaks in the ship plumes, because the duration of the plume
415 itself was of the order of a few minutes. This was the reason for shortening the response time of the analyzers by increasing the flow rate from the nominal flow and shortening the integration time, which then made it possible to increase the data collecting frequency.

As seen from Supplementary Fig. S4, major factors influencing the accuracy of calculating the emission peak area are the difference of the response time between the SO₂ and CO₂ analyzers, but also the frequency of data collection. The Picarro
420 G2301 CO₂ analyzer is clearly faster than the UV-Fluorescence SO₂ analyzers, which are designed for air quality measurements to meet the requirements of EU regulations. Even when improvements were made to the SO₂ analyzer between the 2011 and 2012 campaigns, the difference in the peak width is clearly seen.

The variation between the 2011 and 2012 campaigns in the calculated FSC from the ships that routinely cruise between Helsinki and Stockholm or Helsinki and Tallinn is used when estimating the uncertainty of the FSC according to Eq. (13). In
425 Fig. 11 the relative expanded uncertainty for the FSC, $U_{\text{FSC}}(\%)$, is shown as a function of peak height concentration of SO₂. Calculation of $U_{\text{FSC}}(\%)$ is made for FSC = 0.1 %, 0.5 % and 1 % fulfilling the requirement according to the regulation at the time of the measurements (FSC = 1 %) but also the regulation which came into power in 2014 (Directive, 2012/33/EU). The uncertainty of the FSC increases rapidly, being 100 % at a peak concentration of 3 ppb for a FSC of 0.1 %, and 5 ppb for a FSC of 0.5 %. When more accurate measurements are required, the peak height concentration of SO₂ should be clearly higher
430 than 5 ppb or 10 ppb for the FSC regulation of 0.1 % or 0.5 %, respectively.

No violation against the regulation was observed for the calculated FSC during the campaigns in 2011 and 2012 (Fig. 12). A typical value for FSC 0.4 % was obtained at an uncertainty of 15 % i.e. $0.40 \pm 0.06 \%$. Also the measurements for defining the FSC were in good agreement with the information given by the ship owners.



5 Conclusions

435 Direct exchange of gaseous compounds and nanoparticles between air and sea interface was studied by micrometeorological
methods. The gas compounds SO_2 , NO , NO_2 , O_3 , and CO_2 , as well as the number concentration of nanoparticles, N_{tot} , were
measured at the small island Harmaja beside the major ship routes to and from the City of Helsinki. The challenges in using
the gradient method turned out to be the disturbance of the flow field due to the fire control tower, the swell causing the
breakdown of the Monin-Obukhov theory, small concentration difference between the measurement heights, and rapid change
440 of the concentration of the pollutants emitted from the ships. In spite of the difficulties associated with the gradient method it
became quite clear that no direct gas exchange across the air-sea interface, negative or positive fluxes occurred, in the case of
nitrogen compounds, ozone or sulfur dioxide. However, the case was slightly different in the case of CO_2 where deposition
but also emission from the seawater occurred, while for nanoparticles deposition was mostly observed. Parallel flux
measurements of CO_2 by the eddy covariance method were also influenced by disturbances at short time frequencies changing
445 the sign of fluxes from positive to negative. However, in spite of the disturbances, the agreement between the two
micrometeorological methods for CO_2 was good. During the second campaign in 2012 eddy covariance measurements
conducted at Harmaja and on the R/V Aranda agreed very well. The measurements of sea surface pCO_2 on R/V Aranda
confirmed that situations of upwelling typically cause positive fluxes.

The measurements for determining the FSC were in good agreement with the information given by the ship owners. The
450 measurement method used to determine the FSC content of marine fuel from the ambient air in connection with the
identification data from AIS gives a clear demonstration of whether the regulations are respected.

The uncertainty analysis of the flux and FSC measurement results was conducted according to the well-known law of
propagation of errors, and following the recipes from the literature (JCGM, 2008). Much effort was expended to build the
uncertainty budget for each of the micrometeorological methods as well as for determining the FSC. The uncertainty budget,
455 pointing out the sources of uncertainties and their contribution on the measurement results, may be conservative, and it may
be improved depending on the selected measurement technique, capabilities of the analyzers, measurement site and the
meteorological situations. In this study, the meteorological situations together with the disturbances of the flow field due to
the location of the measurement mast gave the largest contribution to the uncertainty budget for gases and nanoparticles except
in the case of SO_2 flux. The concentration of SO_2 was close to the detection limit most of the time causing large uncertainty in
460 the result except when emission from a bypassing ship was measured. The uncertainty values of the FSC for the marine fuels
used was acceptable, but challenges arise when these methods are used to determine compliance with the present regulations
(Fig. 11).

To improve the accuracy for determining the FSC based on measurements of the ratio of SO_2 to CO_2 from emission peaks
of ship plumes, development of an instrumentation that can simultaneously measure SO_2 and CO_2 concentration fast enough
465 and with the same order of response time is highly desirable.



Data availability. The data is available at DOI:10.5281/zenodo.4439605.

Supplement. The supplement related to this article is available online.

470

Author contributions. JW and LP designed the concept of the study. JW, LP, TW performed the measurements with the help of TL, JH, TT and MM. HP and KK were responsible for the Aranda measurements and the aspects in the marine boundary layer. HN carried out the OpenForm simulations, J.-PJ provided the AIS data and NO_x emissions from ships (Fig. 1). JW wrote the original manuscript, LP, HP, KK, J.-P.J edited. All authors have read and agreed to the published version of the

475 manuscript.

Competing interests. The authors declare that they have no conflict of interest.

Acknowledgements. The measurements were carried out during the SNOOP project, financed by the Cental Baltic INTERREG
480 IV A Programme 2007–2013 and the Centre for Economic Development, Transport and the Environment (ELY) of Southwest Finland. This project has also received funding from the European Union’s Horizon 2020 research and innovation programme under grant agreement #814893 (SCIPPER project). This work reflects only the authors’ view and INEA is not responsible for any use that may be made of the information it contains. The authors are very grateful to Mr. Aleksi Malinen at Metropolia University of Applied Sciences for help in the measurements and to Ms. Kaisa Lusa and Sisko Laurila at the Finnish
485 Meteorological Institute for help in laboratory calibrations. For revision of the language, the authors are very grateful to Ms. Leena Kahma.

References

- Alföldy, B., Lööv, J. B., Lagler, F., Mellqvist, J., Berg, N., Beecken, J., Weststrate, H., Duyzer, J., Bencs, L., Horemans, B., Cavalli, F., Putaud, J.-P., Janssens-Maenhout, G., Csordás, A. P., Van Grieken, R., Borowiak, A., and Hjorth, J.: Measurements
490 of air pollution emission factors for marine transportation in SECA, Atmos. Meas. Tech., 6, 1777–1791, doi:10.5194/amt-6-1777-2013, 2013
- Businger, J.A.: Evaluation of the Accuracy with Which Dry Deposition Can Be Measured with Current Micrometeorological Techniques, J. Climate and Appl. Meteorol., 25, 1100 - 1124, 1986.
- Businger, J. A., Wyngaard, J. C., Izumi, Y., and Bradley, E.F.: Flux profile relationships in the atmospheric surface layer, J.
495 Atmos. Sci., 28, 181 -189, 1971.
- Cooper, D. A.: HCB, PCB, PCDD and PCDF emissions from ships, Atmos. Environ., 39, 4901–4912, 2005.
- De Leeuw G., Ambelas Skjøth C., Hertel O., Jickells T., Spokes L., Vignati E., Frohn L., Frydendall J., Schulz M., Tamm S., Sørensen L.L., Kunz G.J. Deposition of nitrogen into the North Sea. Atm, Env. 37 Supplement No1, S145 – S165, 2003.



- Directive 1999/32/EC. Sulphur content in Marine fuels.
- 500 Directive 2012/33/EU. Sulphur content in Marine fuels.
- Drennan, W., Donelan, M. A., Madsen, N., Katsaros, K. B., Terray, E., Flagg, C. N.: Directional Wave Spectra from a Swath Ship at Sea, *J. Atmos. Ocean. Technol.*, 11, 896-908, DOI: 10.1175/1520-0426(1994)011<1109:DWSFAS>2.0.CO;2, 1994.
- Drennan, W. M., Graber, H. C., Hauser, D., Quentin, C.: On the wave age dependence of wind stress over pure wind seas, *J. Geophys. Res.*, 108, 8062,8075, doi 1029/2000JC000715, 2003.
- 505 Dyer, A. J.: A review of flux-profile relations, *Boundary Layer Meteorol.*, 1, 363 – 371, 1974.
- Dyer, A. J., Hicks, B. B.: Flux-gradient relationships in the constant flux layer. *Quart. J. R. Met. Soc.* 96, 715-721, 1970.
- Duyzer, J. H., Deinum, G., Baak, J.: The interpretation of measurements of surface exchange of nitrogen oxides: correction for chemical reactions, *Phil. Trans. R. Soc. Lond.* 351, 231 – 248, 1995.
- Haerri, H.-P., Macé, T., Waldén, J., Pascale, C., Niederhauser, B., Wirtz, K., Stovcik, V., Sutour, C., Couette, J., Waldén T.:
- 510 Dilution and permeation methods for the generation of NO, NO₂ and SO₂ calibration gas mixture, *Meas. Sci. Technol.*, 28, 035801, DOI: 10.1088/1361-6501/aa543d, 2017.
- HELCOM Maritime19/5-2.INF "Emissions from Baltic Sea shipping in 2006 – 2018", by Jalkanen, J.-P. and Johansson L: <https://portal.helcom.fi/meetings/MARITIME%2019-2019-582/MeetingDocuments/5-2%20Emissions%20from%20Baltic%20Sea%20shipping%20in%202006%20-%202018.pdf>, last access 4.4.2020.
- 515 Hongisto, M. and Joffre, S.: Meteorological and climatological factors affecting transport and deposition of nitrogen compounds over the Baltic Sea, *Boreal Env. Res.*, 10, 1–17, 2005.
- Hongisto, M.: Impact of the emissions of international sea traffic on airborne deposition to the Baltic Sea and concentrations at the coastline, *Oceanologia*, 56, 349-372, 2014.
- Högström, U., Sahlée, E., Drennan, W. M., Kahma, K. K., Smedman, A.-S., Johansson, C., Pettersson, H., Rutgersson A.,
- 520 Tuomi, L., Zhang, F., Johansson, M.: Momentum fluxes and wind gradients in marine boundary layer – a multi-platform study, *Boreal Env. Res.*, 13, 475-502, 2008.
- Högström, U., Rutgersson, A., Sahlée, E., Smedman, A.-S., Hristor, T., S., Drennan, W. M., Kahma, K. K.; Air-sea interaction features in the Baltic Sea and at a Pacific trade-wind site: an Inter-comparison study, *Boundary-Layer Meteorol.*, 147, 139-163, DOI 10.1007/s10546-012-9776-8, 2013.
- 525 Högström, U., Sahlée, E., Smedman, A.-S., Rutgersson, A., Nilsson, E., Kahma, K.K., Drennan, W. M. J., Surface Stress over the Ocean in Swell-Dominated Conditions during Moderate Winds, *J. Atmos. Sci.*, 72, 4777–4795, 2015, DOI: 10.1175/JAS-D-15-0139.1.
- IMO: International Maritime Organisation, Guidelines for the Control and Management of Ships' Ballast Water to Minimise the Transfer of Harmful Aquatic Organisms and Pathogens,
- 530 <http://www.imo.org/en/KnowledgeCentre/IndexofIMOResolutions/Assembly/Documents/A.868%2820%29.pdf>, last access 17.9.2020.
- JCGM; Evaluation of measurement data – Guide to the expression of uncertainty in measurement, JCGM, 100, 2008.



- Jalkanen, J.-P., Brink, A., Kalli, J., Pettersson, H., Kukkonen, J., and Stipa, T.: A modelling system for the exhaust emissions of marine traffic and its application in the Baltic Sea area, *Atmos. Chem. Phys.*, 9, 9209-9223, 2009.
- 535 Johansson, L., Jalkanen, J.-P.: Emissions from Baltic Sea Shipping in 2015, <https://helcom.fi/baltic-sea-trends/environment-fact-sheets/maritime-activities/emissions-from-baltic-sea-shipping-in-2015/>, 2016, last access 17.9.2020.
- Johansson J.E., Gauss M., Schulz M., Jalkanen J.-P., and Hagerli H.: Effects of global ship emissions on European air pollution levels. *Atmos.Chem.Phys.*, 20, 11399 – 11422, 2020.
- Kahma, K. K., Donelan, M. A., Drenman, W. M., Terray, E. A.: Evidence of energy and momentum flux from swell to wind, 540 *J. Phys. Oceanogr*, 46, 2143-2156, <https://doi.org/10.1175/JPO-D-15-0213.1>, 2016.
- Kaimal, J.C., Finnigan J. J.: *Atmospheric boundary layer flows: their structure and measurement*, Oxford University Press, New York, 1994.
- Keskinen, J., Pietarinen, K., Lehtimäki, M.: Electrical low pressure impactor, *J. Aerosol Sci.*, 23, 353-360, 1992.
- Kramm, G., Müller, H., Fowler, D., Höfken, K.D., Meixner, F.X., Schaller, E.: A modified Profile Method for Determining 545 the Vertical Fluxes of NO, NO₂, Ozone and HNO₃ in the Atmospheric Surface Layer, *Journal of Atmospheric Chemistry*, 13, 265 – 288, 1991.
- Lehmann, A., Myrberg, K.: Upwelling in the Baltic Sea - a review, *Phys. Chem. Earth, B* 25, 183-189, 2008.
- Lenschow, D. H., Kristensen, L.: Uncorrelated noise in turbulence measurements, *J. Atmos. Ocean. Tech.*, 2, 68–81, 1985.
- Lenschow, D., Delany, A. C.: An analytical Formulation for NO and NO₂ Flux Profiles in the Atmospheric surface Layer, 550 *Journal of Atmospheric Chemistry*, 5, 301 – 309, 1987.
- Lenschow, D. H., Mann, J., Kristensen, L.: How long is long enough when measuring fluxes and other turbulence statistics?, *J. Atmos. Ocean. Tech.*, 18, 661–673, 1994.
- Marjamaki, M., Ntziachristos, L., Virtanen, A., Ristimäki, J., Keskinen, J., Moisio, M., Palonen, M., Lappi, M.: Electrical Filter Stage for the ELPI. Society of Automotive Engineers, SAE Technical Paper 2002-01-0055, 2002.
- 555 Mellquist, J., Beecken, J., Conde, V., Ekholm, J.: Surveillance of Sulfur Emissions from Ships in Danish Waters, Final Report to Danish Environmental Agency, DOI: 10.17196/DEPA.001,2018.
- Moldanová, J., Fridell, E., Winnes, H., Holmin-Fridell, S., Boman, J., Jedynska, A., Tishkova, V., Demirdjian, B., Joulie, S., Bladt, H., Ivleva, N. P., and Niessner, R.: Physical and chemical characterization of PM emissions from two ships operating in European Emission Control Areas, *Atmos. Meas. Tech. Discuss.*, 6, 3931– 3982, doi:10.5194/amtd-6-3931-2013, 2013.
- 560 Norman, M., Parampil, S. R., Rutgersson, A, Sahlée, E.: Influence of coastal upwelling on the air-sea gas exchange of CO₂ in a Baltic Sea Basin, *Tellus B*, 65, 21831, <http://dx.doi.org/10.3402/tellusb.v65i0.21831>, 2013.
- OpenFOAM: <http://www.openfoam.org>, 2020, last access 7.4.2020.
- Panofsky, H. A., Dutton, J. A.: *Atmospheric turbulence - Models and methods for engineering applications*. John Wiley & Sons, Inc., New York, USA, 397 p, 1987.
- 565 Paulson, C. A.: The Mathematical Representation of Wind Speed and Temperature Profiles in the Unstable Atmospheric Surface Layer, *J. Appl. Meteor.*, 9, 857-861, 1970.



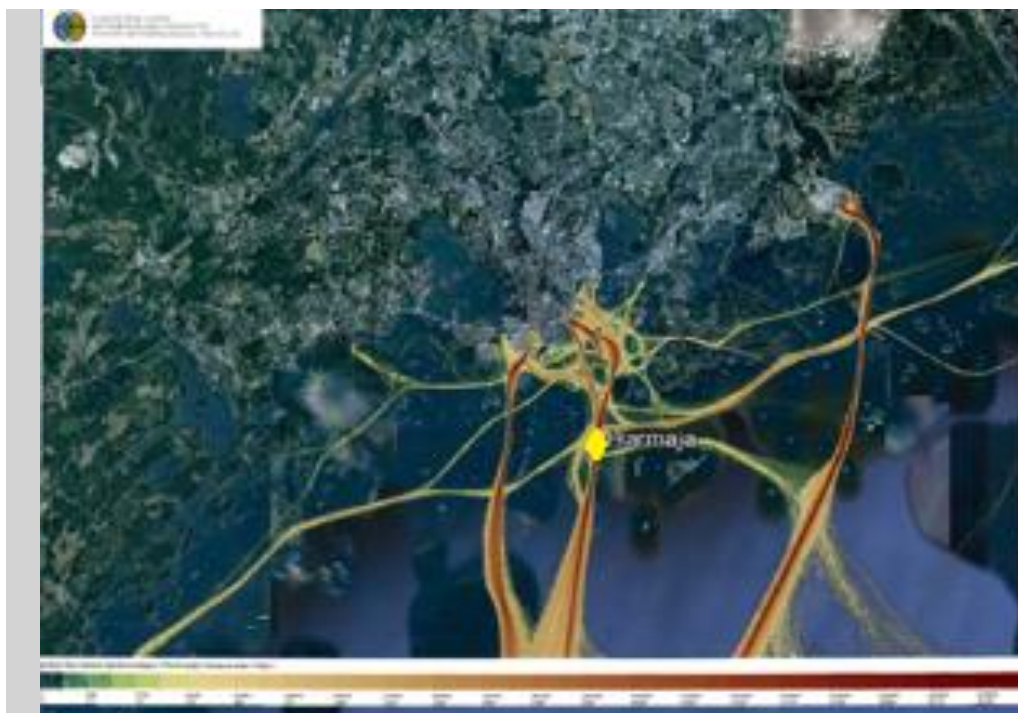
- Petzold, A., Hasselbach, J., Lauer, P., Baumann, R., Franke, K., Gurk, C., Schlager, H., Weingartner, E.: Experimental studies on particle emissions from cruising ship, their characteristic properties, transformation and atmospheric lifetime in the marine boundary layer, *Atmos. Chem. Phys.*, 8, 2387–2403, doi:10.5194/acp-8-2387-2008, 2008.
- 570 Pirjola L., Pajunoja A., Walden J., Jalkanen J.-P., Rönkkö T., Kousa A., Koskentalo T.: Mobile measurements of ship emissions in two harbour areas in Finland, *Atmos. Meas. Tech.*, 7, 149 – 161, 2014.
- Rannik, Ü., Kolari, P., Vesala, T., Hari, P.: Uncertainties in measurement and modelling of net ecosystem exchange of a forest ecosystem at different time scales, *Agr. Forest Meteorol.*, 138, 244–257, 2006.
- Rinne, J. Tuovinen J.-P., Laurila, T., Hakola, H., Aurela, M., Hypen, H.: Measurements of hydrocarbon fluxes by a gradient
575 method above a northern boreal forest, *Agricultural and forest meteorology*, 102, 25 – 37, 2000.
- Seinfeld, J. H., Pandis, S. N.: *Atmospheric Chemistry and Physics: From Air Pollution to Climate Change*, Wiley, 2012.
- Seppälä S., Kuula J., Hyvärinen A.-P., Saarikoski S., Rönkkö T., Keskinen J., Jalkanen J.-P., Timonen H.: Effects of marine fuel sulfur restrictions on particle number concentrations and size distributions in ship plumes at the Baltic sea. <https://doi.org/10.5194/acp-2020-949>.
- 580 Smedman, A., Högström, U., Bergström, H., Rutgersson, A., Kahma, K. K., Pettersson H.: A case-study of air-sea interaction during swell conditions, *J. Geophys. Res.*, 104, 25833 – 25851, 1999.
- Stohl, A., Wotawa, G., Seibert, P., Kromp-Kolb, H.: Interpolation errors in wind fields as a function of spatial and temporal resolution and their impact on different types of kinematic trajectories, *J. Appl. Meteor.*, 34, 2149-2165, 1995.
- Webb, E.K., Pearman, G. I., Leuning R.: Correction of flux measurements for density effects due to heat and water vapour
585 transfer, *Quart. J. Met. Soc.*, 106, 85 – 100, 1980.
- Vila-Guerau de Arellano, J., Duynkerke, P. G., Builtjes, P. J. H.: The divergence of the turbulent diffusion flux in the surface layer due to chemical reactions: the NO-O₃-NO₂ system, *Tellus*, 45B, 23 – 33, 1993.
- Williams, E. J., Lerner, B. M., Murphy, P. C., Herndon, S. C., Zahniser, M. S.: Emissions of NO_x, SO₂, CO and HCHO from commercial marine shipping during Texas Air Quality Study (TexAQS) 2006, *J. Geophys. Res.*, 114, D21306,
590 doi:10.1029/2009JD012094, 2009.
- WMO 2013. WMO/IAEA Meeting on Carbon Dioxide, Other Greenhouse Gases and Related Tracers Measurement Techniques GGMT-2013, GAW report 213, July 2014.
- Yli-Ojanperä, J., Kannosto, J., Marjamäki, M., Keskinen, J.: Improving the nanoparticle resolution of the ELPI, *Aerosol. Air Qual. Res.*, 10, 360–366, 2010.



Table 1. Estimated relative expanded uncertainties for the fluxes of gaseous CO₂ and nanoparticles by the GR method, and for CO₂ by the EC method in meteorological situations of stationary (U_{Stat.Met.}) and not stationary (U_{Prev.Met.}). More details of the uncertainty budget are presented in Supplementary Table S1. The uncertainty values are given at the median flux values.

Flux	Method	Flux (median)	U _{Stat.Met.}	U _{Prev.Met.}
F _{CO2}	EC	-0.0036 mg m ⁻² s ⁻¹	30.0 %	60.0 %
F _{CO2}	GR	-0.0036 mg m ⁻² s ⁻¹	24.9 %	36.4 %
F _{Ntot}	GR	-229.1 cm ⁻³ m s ⁻¹	30.8 %	40.7 %

600

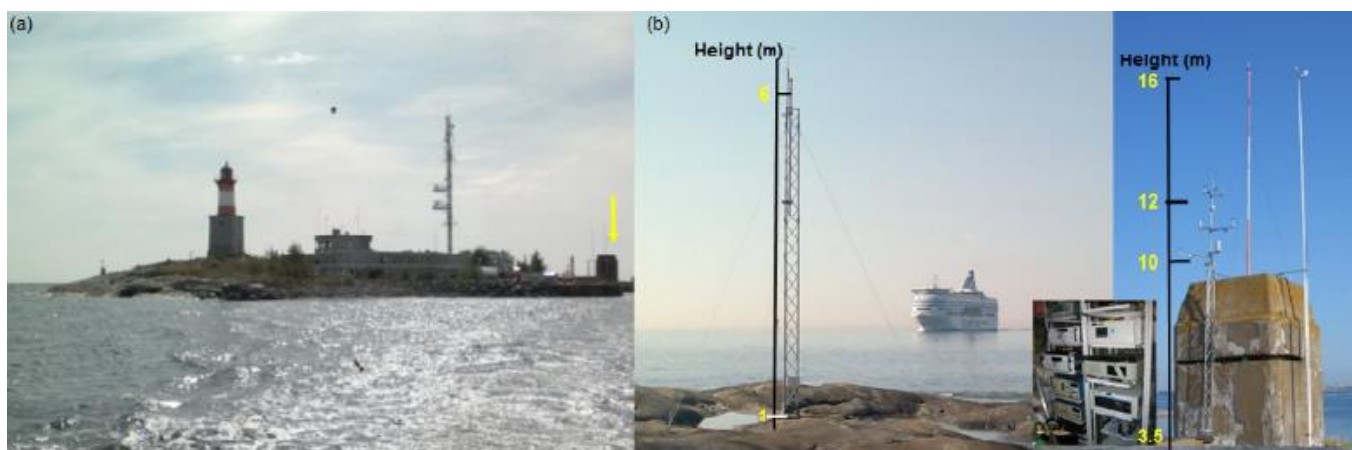


605

Figure 1. Ship routes to the harbours of Helsinki and NO_x emissions. Harmaja Island is marked by the yellow star. Background map was provided by Landsat-8 and US Geological Survey.



610



615

Figure 2. a) Harmaja island. The yellow arrow points to the measurement tower. b) Measurement instrumentation was installed in racks inside the fire control tower. The mast on the right includes all the measurement probes (wind and temperature probes and sample intakes) for the gradient and eddy covariance methods during the 2011 campaign, whereas the mast on the left includes the probes and sample inputs for the eddy covariance method and for measuring gas and particle concentration during the 2012 campaign. Both masts faced the open sea. The masts stood approximately 20 m from the shoreline and 3.5 m above MSL in 2011, and 3 m from the shoreline and 1 m above MSL in 2012. The official weather mast of the FMI is located by the side of the tower (right-side mast, 16.6 m).



620

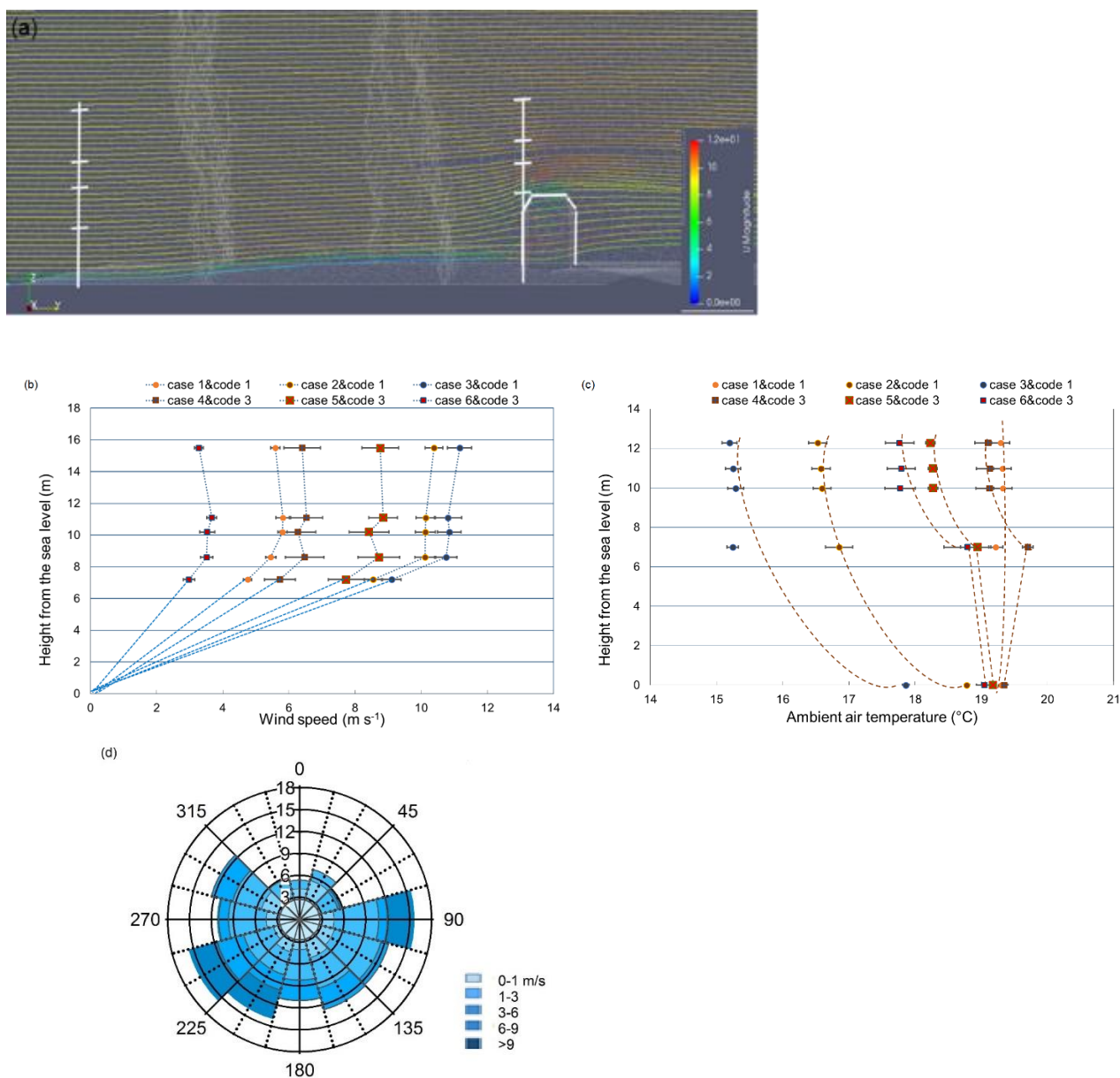


Figure 3. a) The actual measurement heights were reduced to corresponding heights over the open sea surface with a flow dynamics program. b) Mean wind speed profiles over 2 to 3 hours are presented at different heights in the wind direction sector from 150° to 270°. The dots represent the situations of no swell (code 1), while the squares represent cases of swell (code 3). The error bars show the standard deviation of the wind speed over the average period at the respective heights. c) Hourly mean temperature profiles are presented from the same situations as the wind profiles in Fig. 3b. The error bars show the standard deviation of the temperature over the average period at the respective heights. d) Wind rose of direction (scale as %) and wind speed (m/s) at different ranges at the measurement height of 16.6 m.



630

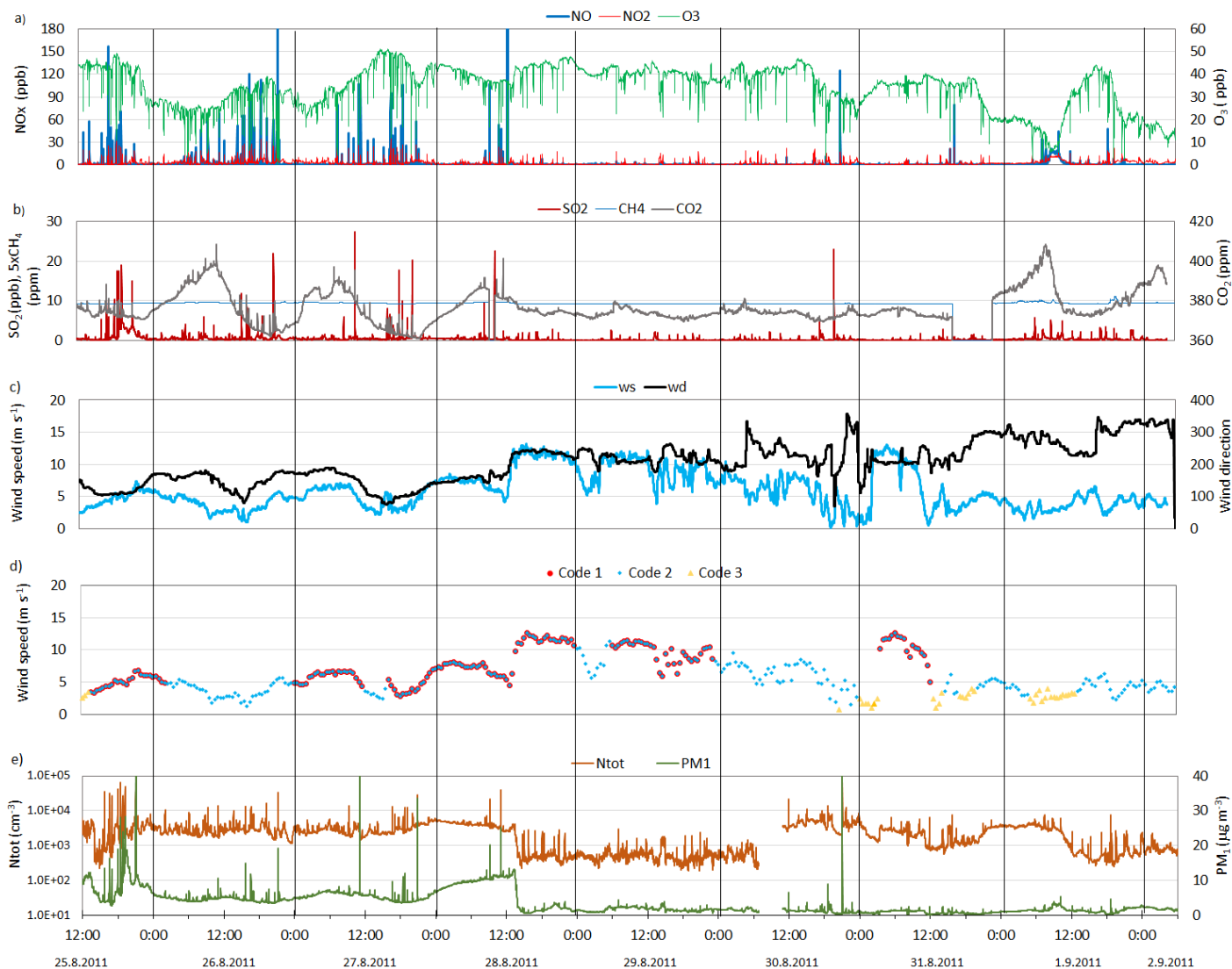
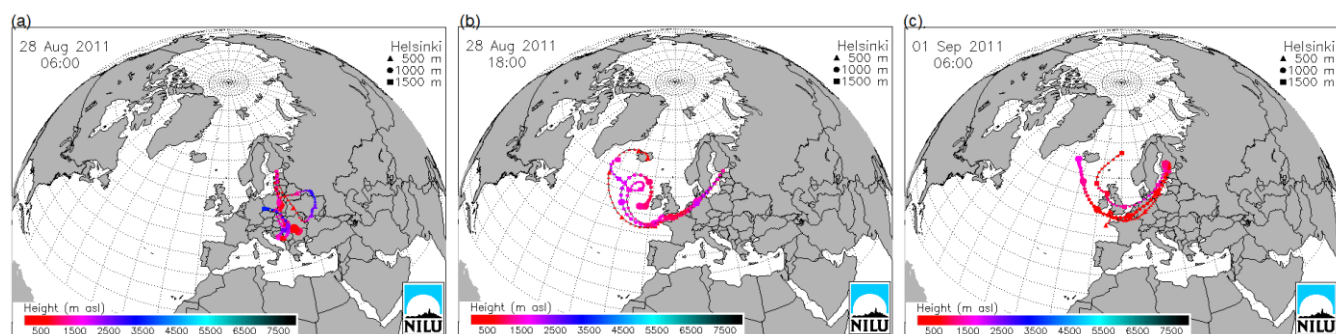


Figure 4. One-minute average concentrations of gaseous (a-b) and particulate (e) matter during 25.8.-2.9.2011. Also shown are the wind speed and wind direction (c), and the wind speed (d) in different situations regarding the M-O theory, i.e. codes 1 to 3. The data in (d) were averaged over 30 minutes.

635



640 Figure 5. Selected airmass trajectories 28.8. at 6 am (a) and at 6 pm (b), and 1.9. at 6 am (c) during our campaign of 2011. The times are given in UTC, whereas our data sets are given in EET (UTC+2).

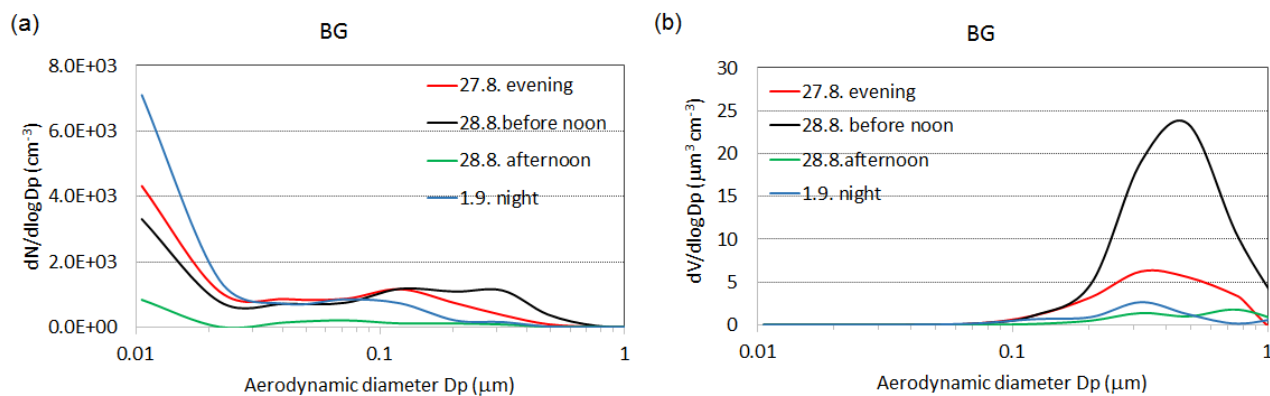
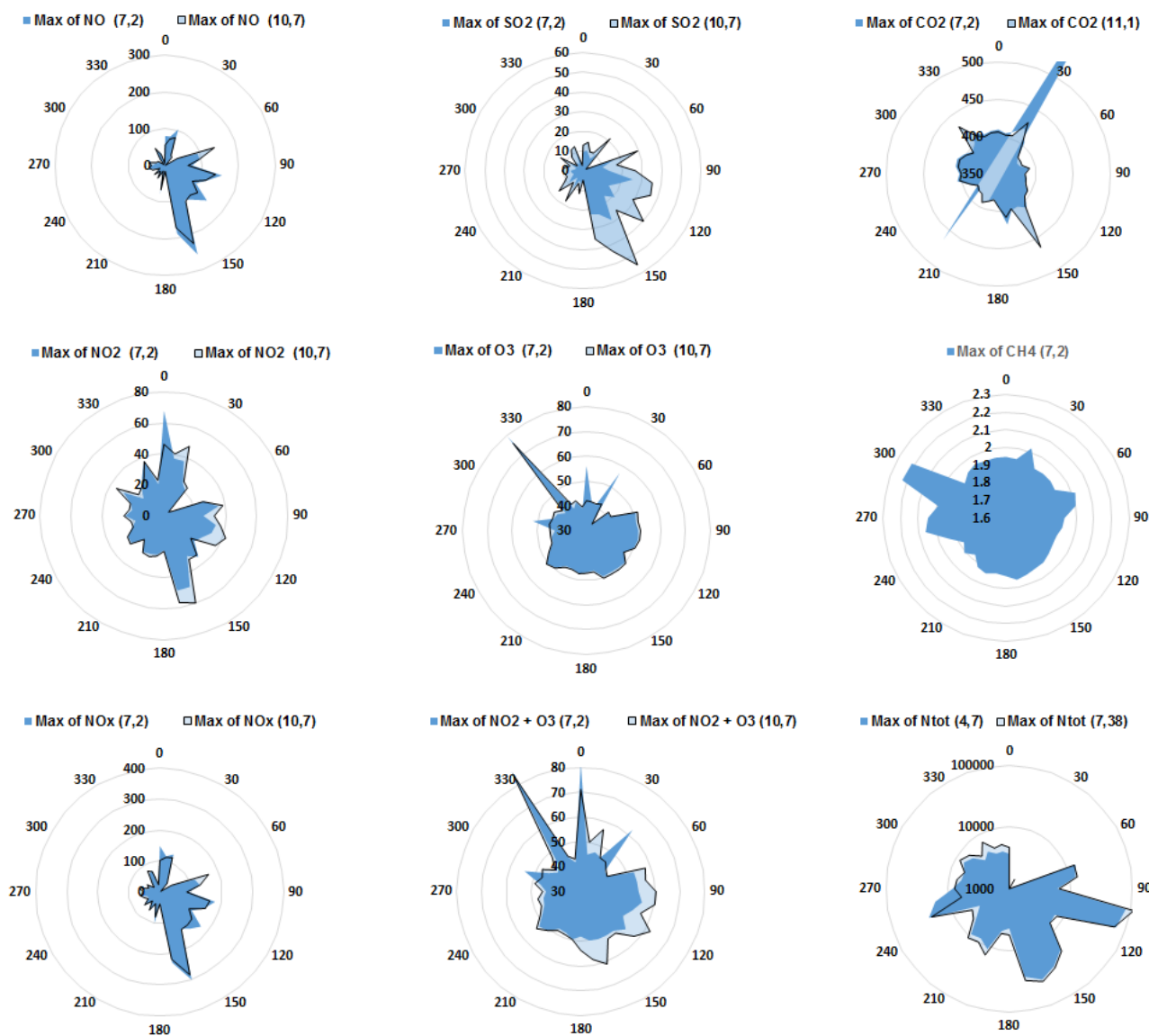
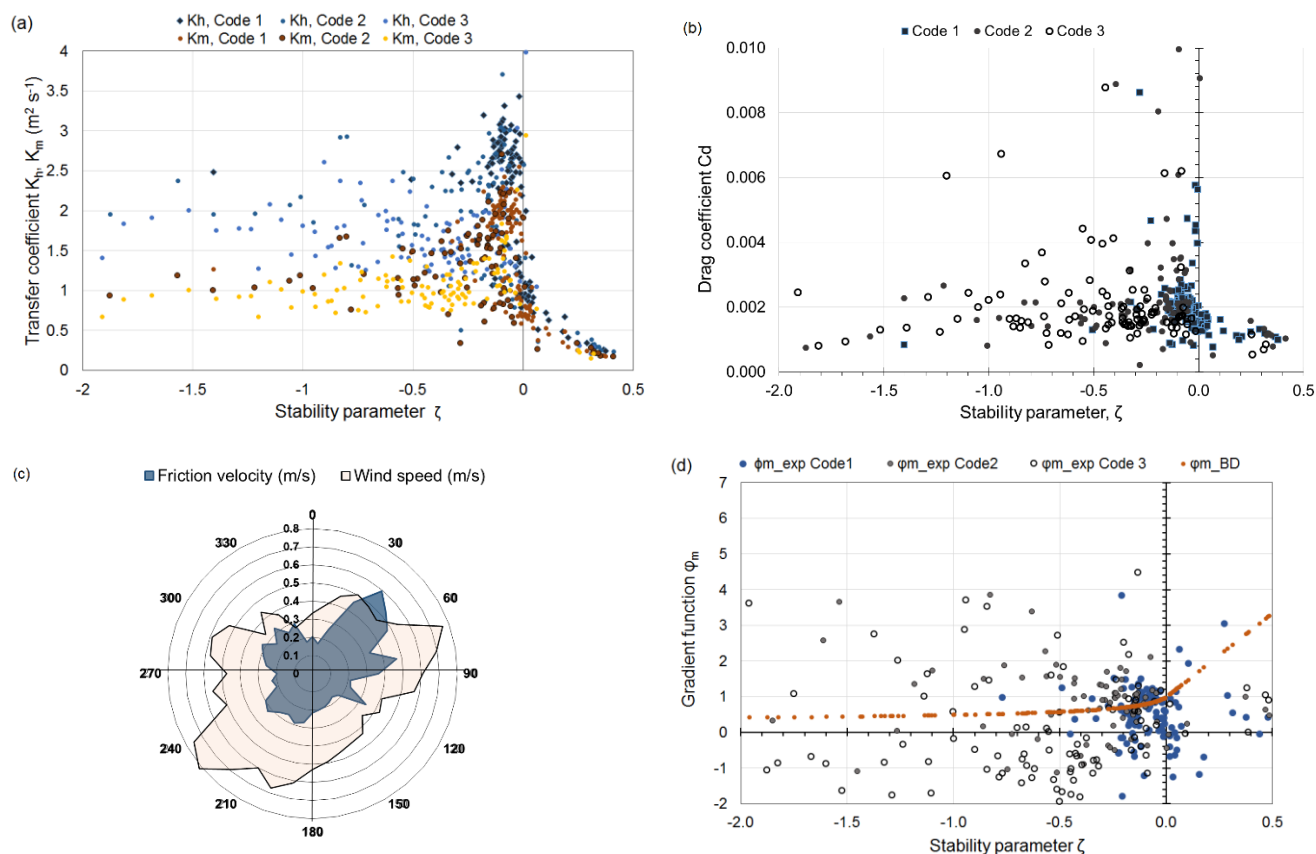


Figure 6. Number (a) and volume (b) size distributions of background particles.



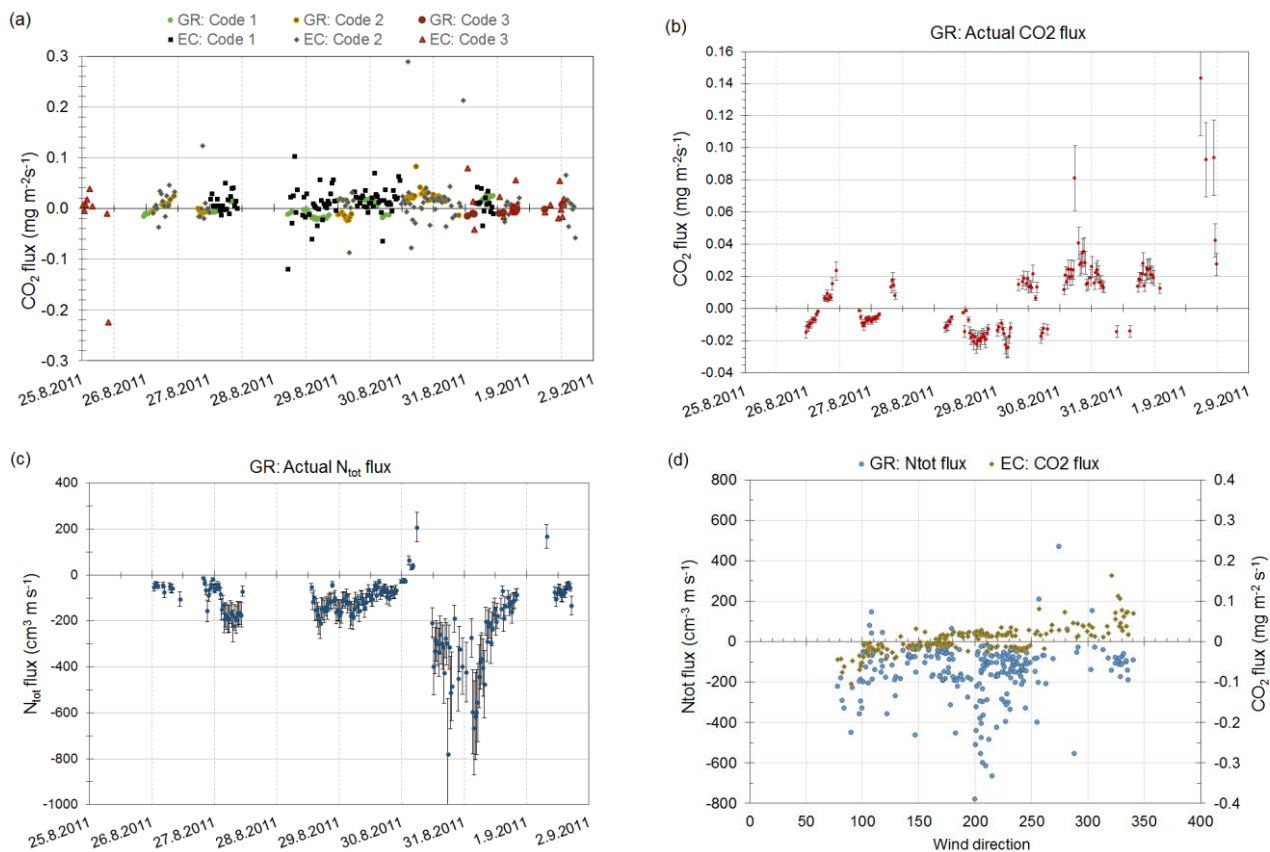
650 Figure 7. Roses of the maximum gaseous concentrations of nitrogen oxides (NO, NO₂, NO_x) in ppb, oxidants O₃ and NO₂+O₃, as well as SO₂ in ppb, and CH₄ and CO₂ in ppm. Also shown are the roses of particle concentrations N_{tot} in #/cm³. All roses, except for CH₄, were plotted from the two heights; the corrected heights (m) are given in parentheses above the roses.



655

Figure 8. a) The eddy diffusivity coefficients K_h (blue) and K_m (brown) as a function of stability at height 12.28 m and with wave codes 1 to 3. b) The friction velocity by sonic anemometer as a function of the stability parameter at 11.1 m height with codes 1 to 3. c) The rose of friction velocity and wind speed as averages over the wind sector. d) The gradient functions from the experiments (ϕ_{m_exp}) at the 15.5 m altitude and from the Businger - Dyer formula (ϕ_{m_BD}) at the wind sector from 150° to 270° and wind speeds $w_s > 3$ m/s for wave codes

660 1 to 3.



665 Figure 9. Time series of 30 min fluxes for CO₂ (mg m⁻² s⁻¹) by the GR and EC methods in different wave conditions (codes 1 to 3) (a), for CO₂ (b) and N_{tot} (c) by the GR method with their uncertainties. The data in (b) and (c) include only events in the wind sector between 150° and 270° and with no swell (codes 1 and 2). In (d) the fluxes of CO₂ and N_{tot} are presented as a function of wind direction (codes 1 to 3).



670

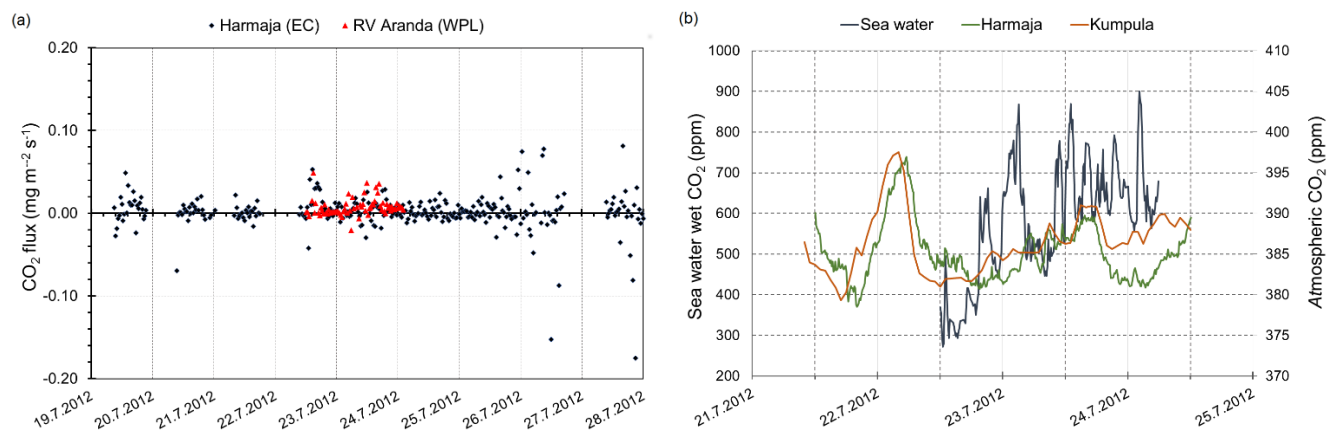


Figure 10. a) Time series of CO₂ fluxes in 2012 at Harmaja and at the R/V Aranda. b) CO₂ concentration in the seawater from R/V Aranda and in the atmosphere at Harmaja and at the urban background monitoring station SMEAR III in Kumpula, Helsinki.



675

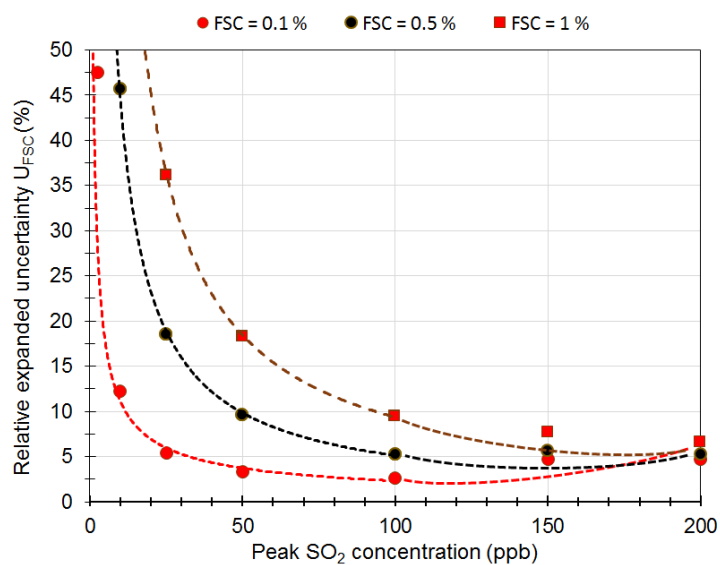


Figure 11. The expanded uncertainty of FSC, U_{FSC} (%), as a function of SO_2 peak height concentration for three FSC limits: 0.1 % (red circle), 0.5 % (black circle) and 1 % (red square).



680

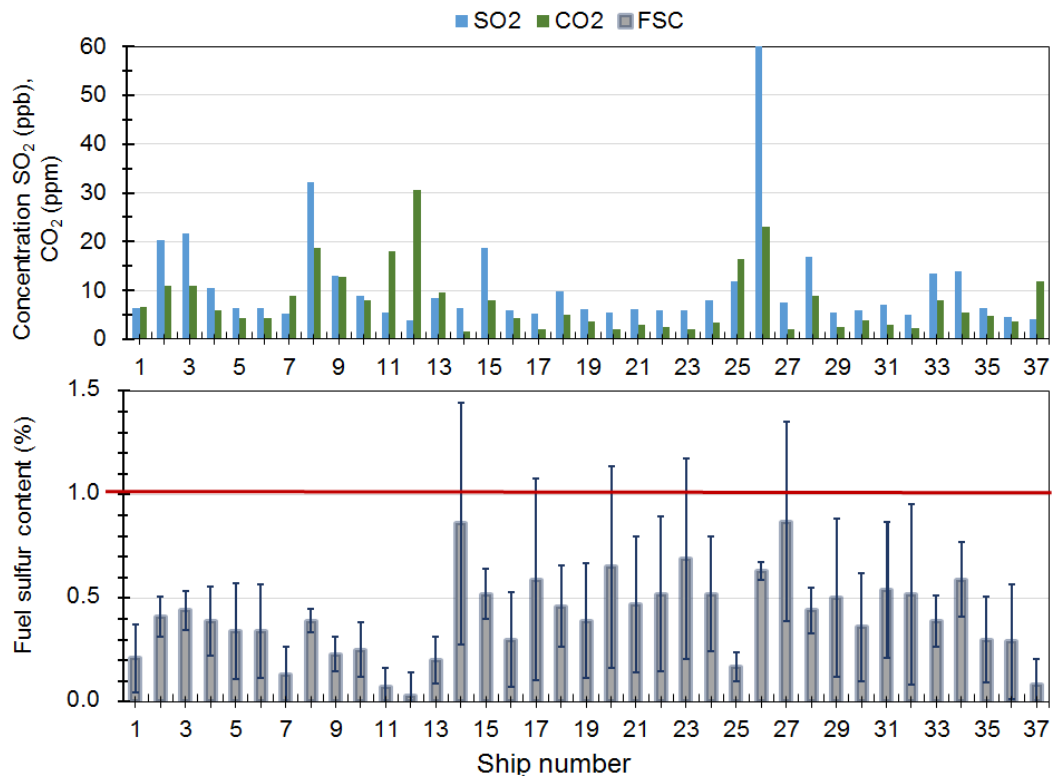


Figure 12. Peak height concentrations of SO₂ and CO₂ from a ship emission plume and calculated FSC with the expanded uncertainty U_{FSC} during a short time period of the 2012 measurements. The red line represents the FSC = 1 % limit following the regulation (Directive 1999/32/EC). All the ships complied with the regulation.